Original paper

Molybdenum isotopic composition of molybdenite and the fertility potential of the Ekomédion U–Mo prospect, SW Cameroon

Victor Fonabe EMBUI[1,2]*, Cheo Emmanuel SUH[3,4], Bernd LEHMANN[5], Lukáš ACKERMAN[6,7]

[1] *Ore Treatment Laboratory, Institute of Geological and Mining Research (IRGM), P.O. Box 4110, Yaoundé, Nlongkak, Cameroon*

[2] *Department of Mining and Mineral Engineering, National Higher Polytechnic Institute, University of Bamenda, P.O. Box 39, Bambili, North West Region, Cameroon; embuivictor@gmail.com*

[3] *Department of Geology, University of Buea, P.O. Box 63, Buea, South West Region, Cameroon*

[4] *Department of Geology, Mining and Environmental Science, University of Bamenda, P.O. Box 39, Bambili, Cameroon*

[5] *Mineral Resources, Technical University of Clausthal, Adolph-Roemer-Str 2A 38678 Clausthal-Zellerfeld, Germany*

[6] *Institute of Geology of the Czech Academy of Sciences, Rozvojová 269, 165 00 Prague 6, Czech Republic*

[7] *Czech Geological Survey, Geologická 6, 150 00 Prague 5, Czech Republic*

* *Corresponding author*

We present Mo isotope data for molybdenite from the Ekomédion U–Mo prospect, SW Cameroon, a Late Neoproterozoic granite–pegmatite–quartz vein system. Disseminated and veinlet-controlled molybdenite in granite and pegmatitic pods yields a narrow range of δ^{98}Mo values from -0.06 to $+0.24$ ‰, with two overlapping populations of $+0.03 \pm 0.07$ ‰ (n=4) in granite, and slightly heavier of $+0.11 \pm 0.10$ ‰ (n = 5) in pegmatite. By contrast, molybdenite from a quartz–muscovite vein has an isotopically heavy δ^{98}Mo value of $+1.61$ ‰. We interpret this trend from granite through pegmatite to vein system towards isotopically heavy Mo to reflect the fractionation of an evolving magmatic–hydrothermal system. Furthermore, the LREE-enriched bulk-rock patterns with largely negative Eu anomalies and the overall enrichment of HREE in zircon indicate plagioclase fractionation as the dominant petrogenetic process during melt evolution. Furthermore, the presence of accessory ilmenite indicates relatively reducing conditions of the melt system, unfavorable for significant Mo accumulation. Therefore, the Ekomédion granite system seems to have limited economic potential for molybdenum despite the advanced degree of magmatic evolution.

1. Introduction

Most of the world's Mo resources are hosted by Cenozoic porphyry systems, especially in the western part of North and South America and in Cretaceous porphyry Mo deposits in South and NW China (Chen et al. 2002; Li et al. 2012; Zhang et al. 2014; Sun et al. 2015; Zhang et al. 2022). On the other hand, economic Mo accumulations in Precambrian and Phanerozoic rocks are sparse, and the economic potential of these occurrences remains unexplored.
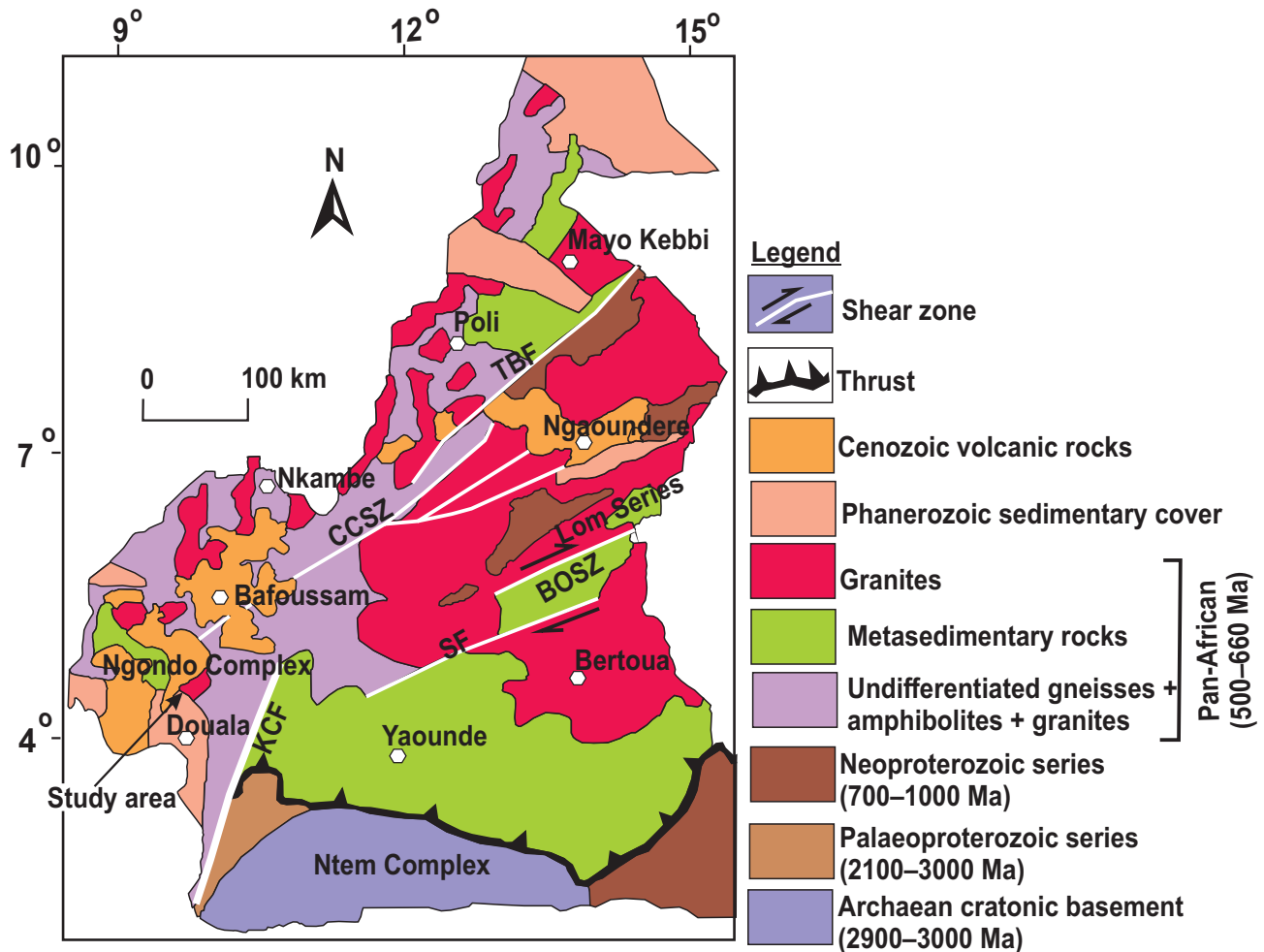
Molybdenum mineralization has been identified in the Pan-African granite of Cameroon. However, little attention has been paid to this Mo deposit, which occurs in association with U within the Ekomédion prospect in SW Cameroon (Mosoh Bambi et al. 2012, 2013; Embui et al. 2020). Therefore, the potential source of Mo and U and the processes leading to their accumulation within the Ekomédion prospect are poorly understood.

In the past years, molybdenum isotope composition expressed as δ^{98}Mo $\{\delta^{98}$Mo (‰) = $[(^{98}\text{Mo}/^{95}\text{Mo})_{\text{sample}}/(^{98}\text{Mo}/^{95}\text{Mo})_{\text{standard}} - 1] \times 1000\}$ has been shown to display

an up to ~2 ‰ isotopic fractionation in high-temperature molybdenite from Cenozoic porphyry deposits (Johnson and Beard 2006; Hannah et al. 2007; Mathur et al. 2010; Shafiei et al. 2015; Breillat et al. 2016; Yao et al. 2016; Li et al. 2019). These variations in δ^{98}Mo can be used to track the evolution of the ore fluids at and below the magmatic–hydrothermal transition (Hannah et al. 2007; Mathur et al. 2010; Greber et al. 2011, 2014; Shafiei et al. 2015).

Kendall et al. (2017) have shown that Mo isotopic compositions of molybdenite can play a major role in revealing conditions and processes of Mo transport and the precipitation of molybdenite. However, the major controlling factors of such fractionation processes, such as phase separation, conversion of Mo species, fluid cooling and redox change, are still debated (Hannah et al. 2007; Greber et al. 2014; Shafiei et al. 2015; Yao et al. 2016; Willbold and Elliott 2017; Wille et al. 2018; Chang et al. 2020; Kaufmann et al. 2021).

Local magmatic–hydrothermal processes are controlled by regional-scale features of melt fertility and melt evolution. Concerning molybdenum mineralization, fer-

Fig. 1 Geologic map of Cameroon showing the position of the area of study in the SW part of Cameroon along the Central Cameroon Shear Zone (CCSZ; modified after Mosoh Bambi et al. 2013; Embui et al. 2020); SF = Sanaga Fault, KCF = Kribi–Campo Fault, TBF = Tcholliré–Banyo Fault, BOSZ = Betaré–Oya shear Zone.

tile melts are assumed to be more oxidized and hydrous (e.g., common I-type granitic intrusions), while infertile melts include the relatively reduced S- and A-type and relatively dry A- and I-type magmas (Ishihara 1981). In this respect, the redox state and water content of magma are believed to be the major factors responsible for the fertility of magma and its ore potential. The studies of Blevin (2004), Loucks (2014), Dilles et al. (2015), Lu et al. (2016) and Li et al. (2019) have shown that zircon serves as a valuable indicator of these factors during magma ascent, and its trace-element characteristics can fingerprint the igneous physicochemical conditions. For example, studies by Ballard et al. (2002) and Dilles et al. (2015) have revealed that fertile magmas linked to Cu mineralization contain zircon that yields characteristic high $Ce^{4+}/Ce^{3+} > 300$ and $Eu/Eu^* > 0.3$. Lu et al. (2016) and Li et al. (2019) have illustrated the effectiveness of zircon trace-element ratios such as Dy/Yb, Eu/Eu* and

(Eu/Eu*)/Y as proxies for the water content of melts. Additionally, whole-rock trace-element compositions provide further constraints on melt fertility with implications for mineral exploration (Lu et al. 2016).

In this contribution, we present field evidence of mineralization, $\delta^{98}Mo$ isotopic data for a suite of molybdenite samples from two-mica granite, pegmatite and penetrating quartz vein of the Ekomédion U–Mo prospect in the context of previously documented field relationships and whole-rock geochemistry (Mosoh Bambi et al. 2012), geochronology (age of granitic intrusions and molybdenite) as well as petrogenetic processes (Mosoh Bambi et al. 2013; Embui et al. 2020). The interpretation of the new Mo isotopic dataset is accompanied by a re-assessment of zircon and whole-rock trace-element data previously published by Embui et al. (2020) in order to provide new insights into the economic potential of the district with respect to Mo.

2. Geological setting

2.1. Regional geology

The orogenic assemblage of Cameroon consists of three major geotectonic units (Fig. 1): (i) Archean–Paleoproterozoic basement gneiss, migmatite and granulite with available ages ranging from ca. 3.09 to 2.49 Ga (e.g., Caen-Vachette 1988; Van Schmus et al. 2008; Chombong and Suh 2013; Chombong et al. 2017), (ii) Meso- to Neoproterozoic volcano-sedimentary sequences that were deformed and metamorphosed to various degrees and yield zircon detrital U–Pb ages from ~1100 to 950 Ma (Toteu et al. 2006), and (iii) Pan-African granitic rocks that intruded the (i–ii) units at ~680–520 Ma (e.g., Asaah et al. 2015; Ateh et al. 2017; Li et al. 2017; Embui et al. 2020) (Fig. 1).

Within the Mayo Kebbi area, zircon U–Pb crystallization ages ranging from ~665 to 640 Ma have been reported (Penaye et al. 2006), while in the Bafoussam area, monazite chemical Th–U–Pb dating of two-mica granites yielded ~564–558 Ma (Djouka-Fonkwe et al. 2008). Mosoh Bambi et al. (2013) reported U–Pb ages of 578 ± 4 Ma and 578 ± 11 Ma for monazite and xenotime in two-mica granite and porphyritic granite, respectively, from the Ekomédion area.

The late Neoproterozoic Pan-African Braziliano tectonic belt lies underneath NE Brazil, Central Africa and most of Saharan Africa (Lerouge et al. 2006). This orogenic belt formed due to a collision between the West African and Congo–São Francisco cratons during the assembly of West Gondwana (Trompette 1997). The collision has induced thrusting over the cratonic forelands, anatexis, shearing and doming. In the course of this orogeny, major deformation zones originated all across the Pan-African Braziliano belt (Borborema Province in NE Brazil, Hoggar, Nigeria and Central Africa) that also include the Pre-Mesozoic Central African Shear Zone (CASZ; Njome and Suh 2005) representing a crustal, strike-slip fault system, which extends from central Africa, across the Atlantic, to NE Brazil.

In Cameroon, the CASZ forms a complex network of structures of variable size and magnitude, such as the NE trending structures represented by the Central Cameroon Shear Zone (CCSZ) (Toteu et al. 2006; Ngako et al. 2008) to the north, Sanaga Fault (SF; Kankeu and Greiling 2006) and Bétaré Oya Shear Zone (Kankeu et al. 2009) to the south (Fig. 1). The understanding of the formation, evolution, extent and geometry of these structures remains limited. Nevertheless, Ngako et al. (2008) described the CCSZ as a zone of highly strained rocks that extends across central Cameroon in a NE–SW direction into the northeastern part of Brazil as the Pernambuco Shear Zone (Castaing et al. 1994; Neves et al. 2005). The Neoproterozoic fold belt of Cameroon comprises a migmatitic-gneiss basement intruded by mafic to felsic plutons (including the Ngondo Complex shown in Fig. 1), overlain by Cretaceous to Tertiary bimodal volcanic complexes (Tagne-Kamga 2003). Three Pan-African main geotectonic units are defined in the Cameroon Mobile Belt: the Poli Group in the north, Adamawa-Yade Group (Lom) in the center and Yaoundé Group in the south (Penaye et al. 2006; Pouclet et al. 2007). These terrains are rich in diverse mineralizations, including Au, Ni–Co–Mn, U, Mo, diamond, iron ore, bauxite, Zn, Sb, Sn, Pb, and Ag (Tita and Kaya 2020). The Ekomédion prospect is located in the Ngondo Complex (Fig. 1), within the SW part of the late Neoproterozoic Fold Belt (Mosoh Bambi et al. 2012) developed along the CCSZ.

2.2. Local geology, rock compositions and structural evolution

Within the larger Ekomédion area, paragneiss is the prevailing rock type that was intruded by main-phase porphyritic biotite granite with several granitic sub-intrusions (two-mica granite, microgranite, alkali-feldspar granite; Mosoh Bambi et al. 2012, 2013; Embui et al. 2020) (Fig. 2). These granitic plutons are partially overlain by Cretaceous limestones and sandstones of the Douala sedimentary basin as well as mafic volcanic rocks of the Cameroon volcanic line in southwestern Cameroon (Fig. 1).

In terms of petrography, the two-mica granite that hosts the U and Mo mineralization is composed of quartz (30 vol. %), plagioclase (22 vol. %), K-feldspar (27 vol. %), biotite (10 vol. %) and muscovite (~6 vol. %) and its texture ranges from fine-grained at the western margin to medium-grained in the ore zone and the eastern margin. Accessory minerals include zircon, ilmenite, monazite and apatite. Hydrothermal alteration is expressed by albitization, muscovitization/sericitization, epidotization, chloritization and silicification.

The sampled outcrops reveal variations in the modal proportion of the above primary constituents based on the degree of hydrothermal alteration and mineralization. For example, primary quartz contents decrease to ~15 vol. % in the ore zone, while its abundance increases by ~10 vol. % at the western margin of the granite due to late-stage quartz precipitation. On the other hand, plagioclase illustrates an inverse relationship with quartz, being more abundant in the ore zone (up to 60 vol. %), but decreasing to 18 vol. % at the western margin of the granite. When muscovitization/sericitization is recognized, the muscovite content in the ore zone doubles, while biotite content decreases to ~3 vol. %.

At outcrops, two-mica granite is characterized by fracture sets with variable orientations, some discordant to the foliation of the paragneiss country rock (Mosoh
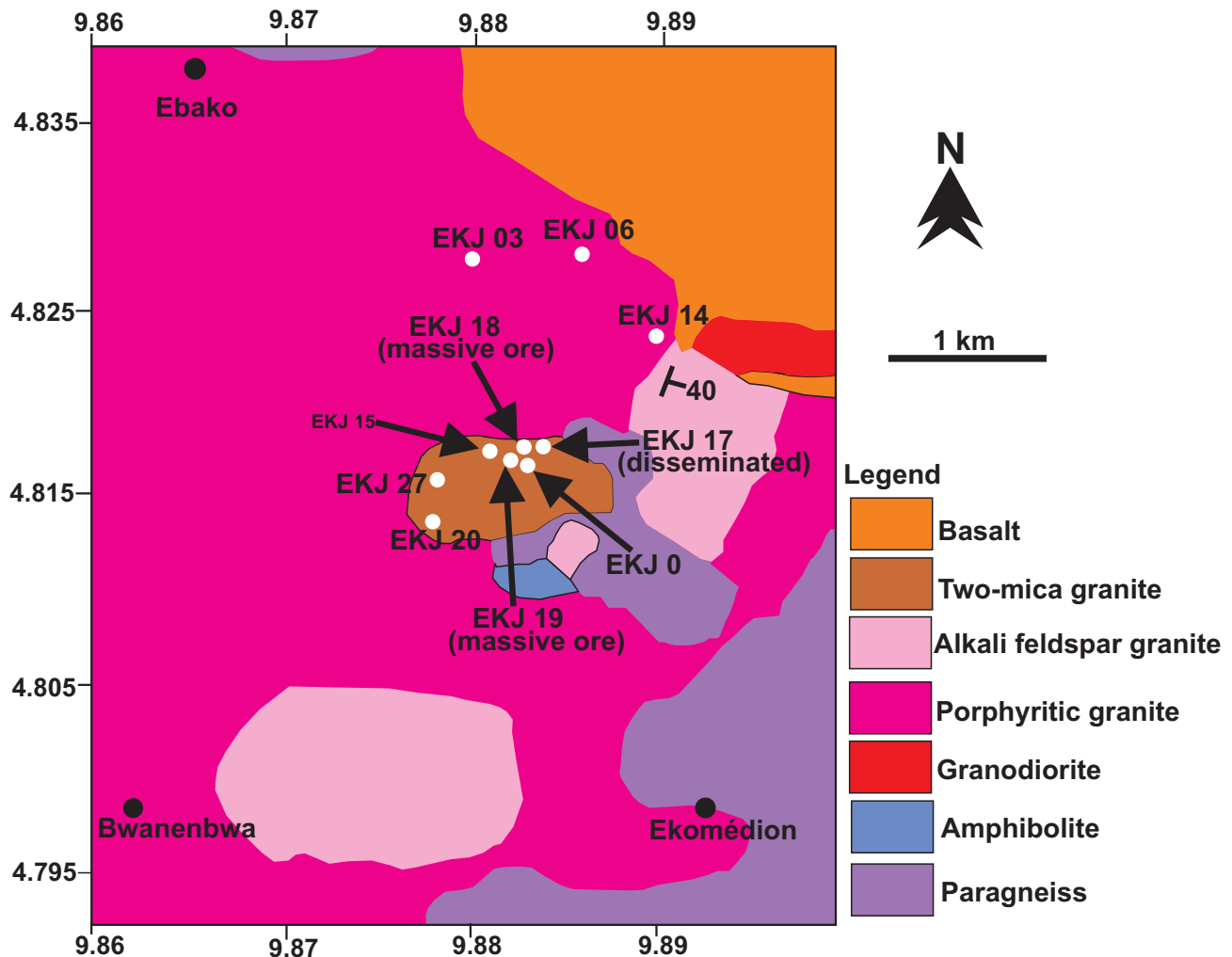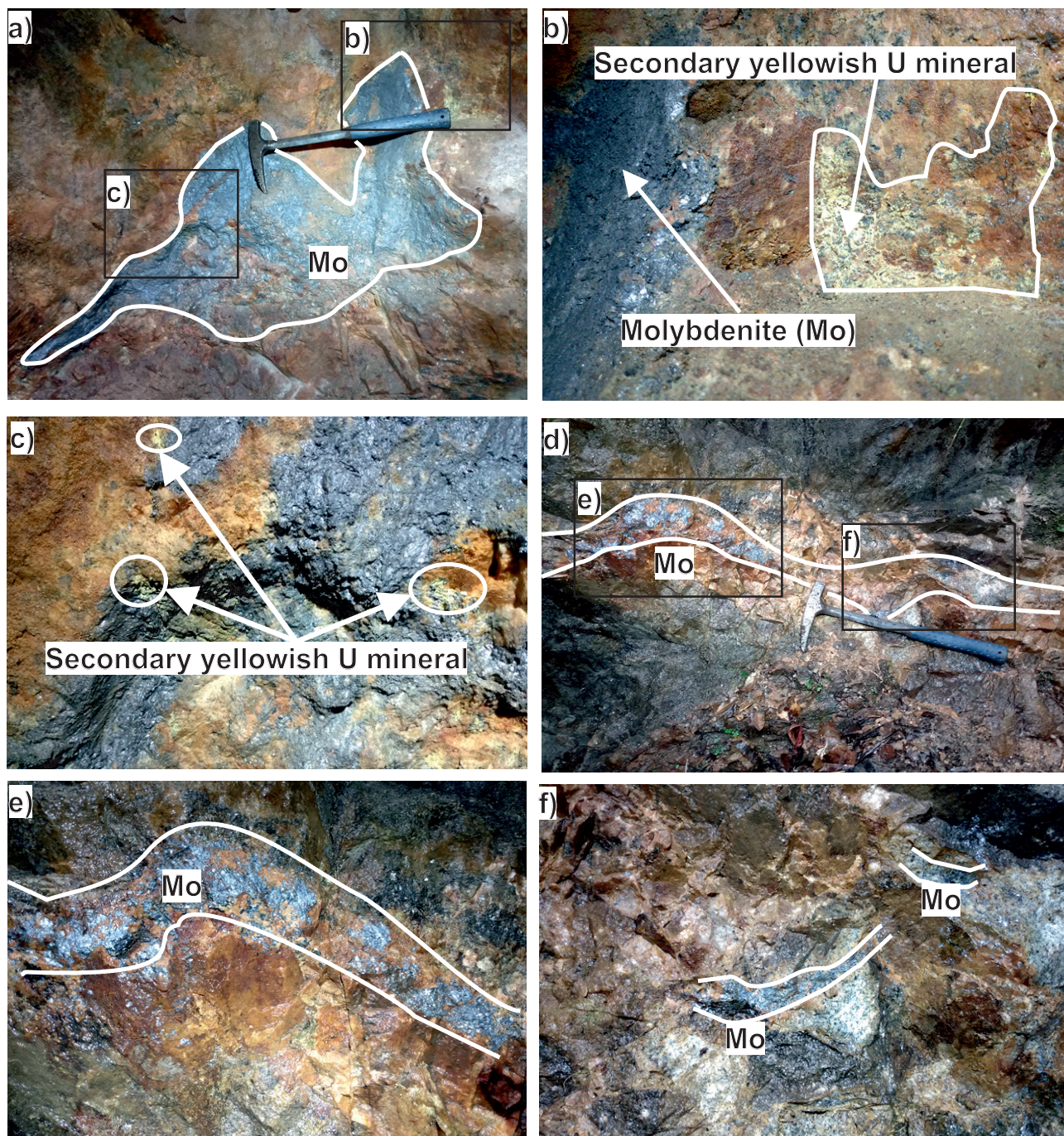
Fig. 2 Detailed geologic map of the Ekomédion prospect (modified after Mosoh Bambi et al. 2012, 2013) with sample locations indicated.

Bambi et al. 2012, 2013; Embui et al. 2020). Additionally, discordant pegmatite and quartz veins are common. In thin sections, the deformed nature of the granite is confirmed by the presence of microstructural features. These microstructural features are localized within the ore zone and are of three types (Mosoh Bambi et al. 2013): (i) early transgranular micro-faults, partly filled with quartz, muscovite and/or Fe-(oxy)-hydroxide with the latter being most likely related to supergene alteration of primary sulfide minerals, (ii) transgranular fractures that are partially filled by hematite or goethite (suspected to have developed from supergene alteration) and muscovite, and (iii) intragranular fractures that are occupied by quartz or muscovite.

3. Analytical methods

Samples were analyzed for their Mo isotopic composition at the joint laboratory of the Institute of Geology at the

Czech Academy of Sciences and the Czech Geological Survey using the double spike technique and Multiple Collector-Inductive Coupled Plasma-Mass Spectrometry (MC–ICP–MS). Given the isotopic heterogeneity reported by Greber et al. (2011) within a single sample of molybdenite, grains from aggregated samples were powdered and homogenized before dissolution. Afterward, about 5 to 20 mg of molybdenite powder was dissolved in 6 mL of *aqua regia* at 120 °C in 15 mL Teflon beakers until complete dissolution. As Mo and S represent the major components of molybdenite, of which S does not interfere with Mo signals (Barling et al. 2001), no Mo separation from the matrix is necessary prior to mass spectrometry analysis (Greber et al. 2011). Therefore, aliquots of solutions obtained by decomposition containing about 10 μg/g of Mo were doped with an appropriate amount of ^{97}Mo–^{100}Mo double spike, heated at 140 °C for 4 hours and then dried. The resulting residues were then dissolved in 1 mL of 0.4 M HNO$_3$–0.05 M HF, and these stock solutions were diluted to about 100 ppb of Mo for

Fig. 3 Outcrop images of massive (a–c) and disseminated (d–f) zones of molybdenite mineralization. Subsections b, c and e, f (black boxes) detailed from (a) and (d), respectively, represent secondary yellowish uranium minerals that are weathering products of uraninite associated with molybdenite (a), as well as, the disseminated Mo mineralization in veinlets (d). Samples EKJ 0 and EKJ 19 in Tab. 1 are from the zone in (a), while EKJ 3, 6 and 14 are from (d). Mo = molybdenite.

subsequent mass spectrometry analyses. The Mo blank for the whole procedure was 5 ng and thus negligible compared to the sample concentration.

The Mo isotopic measurements were carried out on an MC–ICP–MS *Neptune* (Thermo Scientific) at the Czech Geological Survey using the methods described in detail by Gaspers et al. (2020). In brief, the method includes a static collection of 94, 96, 97, 98 and 100 masses of Mo together with monitoring possible isobaric interferences from Zr and Ru using the collection of ^{90}Zr and ^{99}Ru masses, respectively (all on Faraday cups), which were consistently below 1 mV. In addition, the mass-bias correction was applied using the ^{97}Mo–^{100}Mo double spike using five blocks of a nested cascade iteration.

The stable Mo isotopic compositions of molybdenite in this study are reported as δ^{98}Mo relative to NIST 3134 reference Mo solution (Nägler et al. 2014). The method's accuracy was monitored by duplicate analyses of Henderson Mine molybdenite (NIST 8599), yielding δ^{98}Mo values of –0.22 and –0.21 ‰, in excellent agreement with the values of Breillat et al. (2016). The total combined uncertainty of the whole protocol estimated from long-term measurements of NIST 3134 Mo solutions as well as several reference materials (e.g., BHVO-2 and SGR-1b) was ± 0.06 ‰ (2σ) (see Gaspers et al. 2020 for details).
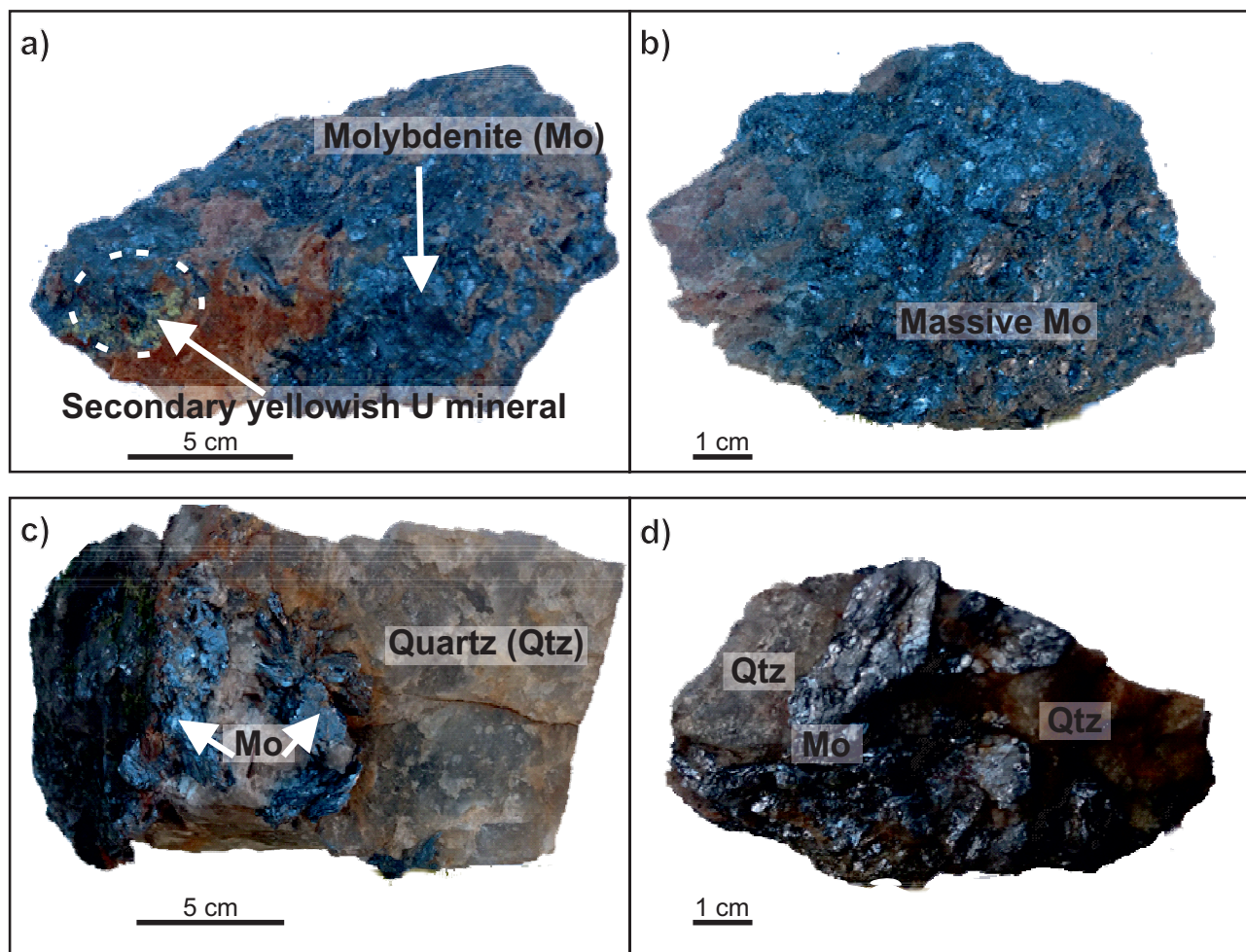
4. Results

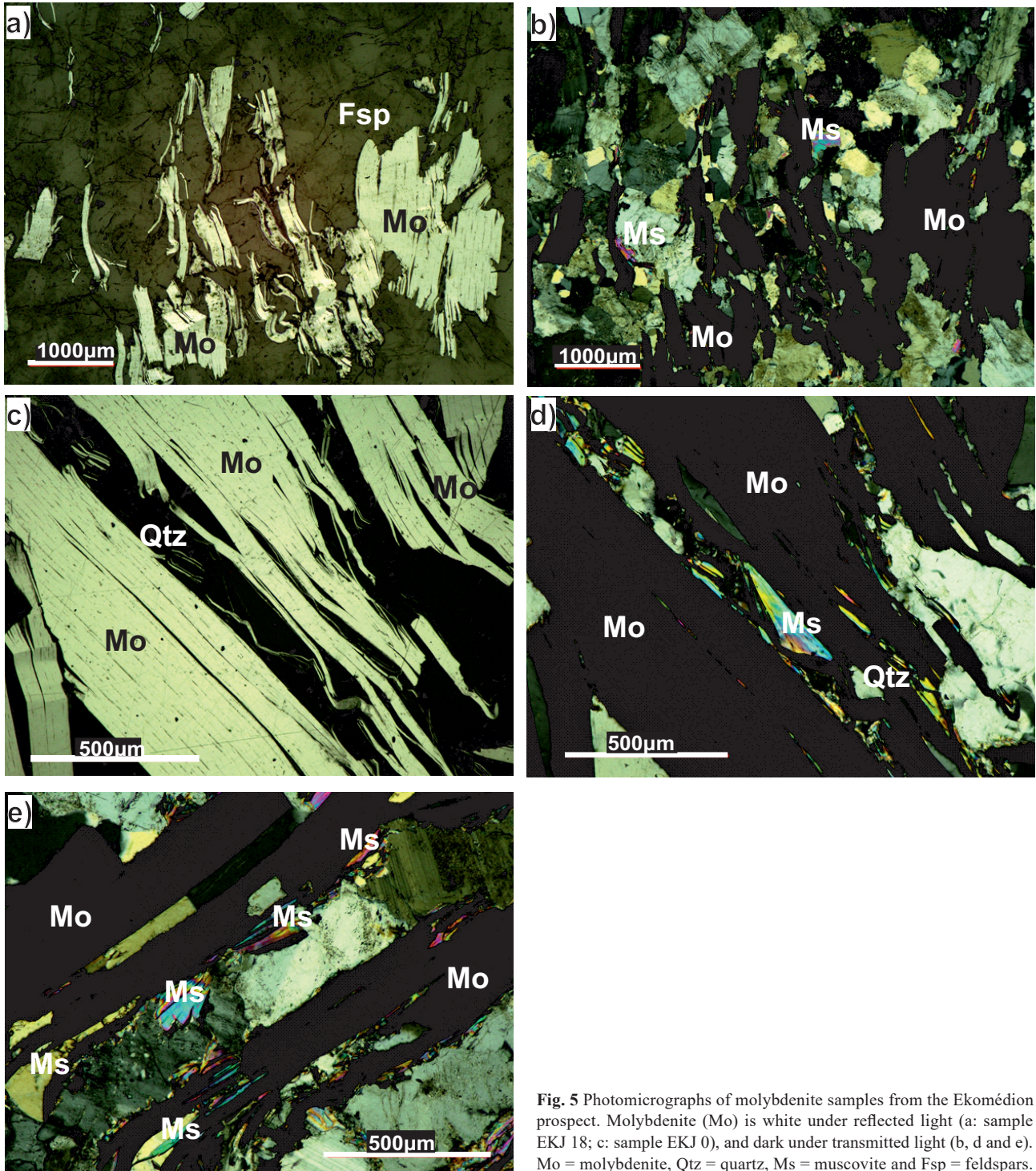### 4.1. Molybdenum mineralization and samples

The U–Mo mineralization of the Ekomédion prospect is represented by uraninite and molybdenite, respectively, concentrated in pegmatitic pods and in quartz veins/veinlets. Molybdenite in the pegmatitic pods hosted by the two-mica granite is either concentrated in ore zones (Figs 3a–c) that indicate an impregnation front (i.e., hydrothermal molybdenite), or it is disseminated within the quartz–feldspar matrix in a dense network of fractures or veinlets. The latter is likely to represent a transitional magmatic–hydrothermal stage (Fig. 3a). Some molybdenite is disseminated in altered fractures and veinlets in the two-mica granite and quartz–muscovite veins in porphyritic granite surrounding the major ore zone (Figs 3d–f). The appearance and texture of hand specimen samples collected within the framework of this study from the major ore zone and a mineralized quartz vein are shown in Fig. 4. Petrography of the ore samples from Ekomédion reveals that molybdenite occurs as sheets intergrown with quartz, K–feldspar and muscovite (Fig. 5).

Ten molybdenite samples were analyzed for their δ^{98}Mo composition (Tab. 1; see Fig. 2 for sample loca-

Fig. 4 Representative hand specimens of the studied samples. Fragments of molybdenite-rich pegmatite pods obtained from the major mineralized ore zone (a, b: samples EKJ 0 and EKJ 19, respectively). Fragments of mineralized quartz vein showing large grains of dispersed molybdenite (c and d: sample EKJ 27). Mo = molybdenite, Qtz = quartz.

Fig. 5 Photomicrographs of molybdenite samples from the Ekomédion prospect. Molybdenite (Mo) is white under reflected light (a: sample EKJ 18; c: sample EKJ 0), and dark under transmitted light (b, d and e). Mo = molybdenite, Qtz = quartz, Ms = muscovite and Fsp = feldspars.

tion). Within this sample set, five samples (EKJ 0, EKJ 17, EKJ 18, EKJ 19 and EKJ 20) were collected from pegmatitic pods hosted by two-mica granite, while four (EKJ 3, EKJ 6, EKJ 14 and EKJ 15) were obtained from outcrops of porphyritic granite and one sample (EKJ 27) from a quartz–muscovite vein where molybdenite forms large pods (Figs 4c–d).

4.2. Molybdenum isotopic composition in molybdenite

The molybdenum isotopic (δ^{98}Mo) compositions of molybdenite from the Ekomédion prospect range from -0.06 to $+1.61$ ‰ (Tab. 1). The samples from granite and pegmatite have a relatively small range (-0.06 to

Tab. 1. The δ^{98}Mo data for the studied molybdenite samples from the Ekomédion prospect, Cameroon

Sample	Host rock	Molybdenite paragenesis	δ^{98}Mo (‰)
EKJ0	Biotite–muscovite granite	Pegmatitic pod	0.15
EKJ17	Biotite–muscovite granite	Pegmatitic pod	0.24
EKJ18	Biotite–muscovite granite	Pegmatitic pod	0.02
EKJ19	Biotite–muscovite granite	Pegmatitic pod	−0.04
EKJ20	Biotite–muscovite granite	Pegmatitic pod	0.18
EKJ3	Biotite granite	Quartz veinlets/disseminated	−0.01
EKJ6	Biotite granite	Quartz veinlets/disseminated	0.13
EKJ14	Biotite granite	Quartz veinlets/disseminated	−0.06
EKJ15	Biotite granite	Quartz veinlets/disseminated	0.04
EKJ27	Biotite–muscovite granite	Quartz–muscovite vein	1.61
Standards			
NIST 8599 Henderson Standard		–	−0.22
NIST 8599 Henderson Standard		–	−0.21

Total uncertainty is 0.06 ‰ (2σ).

0.24 ‰) with a mean δ^{98}Mo of 0.07 ± 0.11 ‰ (n = 9), but two overlapping populations can be distinguished in the box plot of Fig. 6 with a mean δ^{98}Mo of 0.03 ± 0.07 ‰ (n = 4) for granite and 0.11 ± 0.10 ‰ (n = 5) for pegmatite samples. By contrast, an anomalously heavy δ^{98}Mo value of + 1.61 ‰ (Fig. 6; Tab. 1) was obtained for molybdenite from a quartz–muscovite vein (sample EKJ27).

5. Discussion

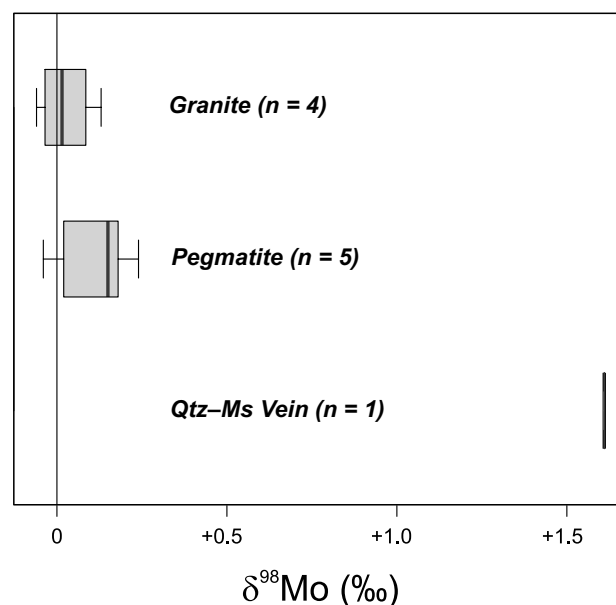## 5.1. Molybdenum isotopic variation and its origin

The δ^{98}Mo values of the Ekomédion molybdenite samples vary in a wide range from − 0.06 to + 1.61‰ (Fig. 6; Tab. 1). In combination with observations gathered from the field and detailed petrography, we assume that this range of isotopic variation can be directly linked to the transitional magmatic–hydrothermal and hydrothermal evolution of the Ekomédion prospect. The textural features of the molybdenite-bearing samples at field and hand specimen scale (Figs 3 and 4) display syngenetic to cross-cutting relationships between molybdenite and their granite and pegmatitic host rocks. Wall-rock alteration within the Ekomédion prospect includes silicification, albitization, sericitization, and chloritization (these were well documented by Mosoh Bambi et al. 2012; Embui et al. 2020), characteristic of a high- to low-temperature overprint. Here, we argue that the wide range of δ^{98}Mo values in the Ekomédion molybdenite reflects the hydrothermal fluid evolution of an evolving granitic system from the transitional magmatic–hydrothermal stage with disseminated mineralization in pegmatitic pods and veinlets (0.07 ± 0.11 ‰ δ^{98}Mo; n = 9) to hydrothermal vein-style mineralization with an advanced degree of Mo isotope fractionation (1.61 ‰ δ^{98}Mo). The disseminated and veinlet-style molybdenite has a Mo isotope composi-

tion little fractionated compared to any igneous system and therefore indicates an origin from a high-temperature and little evolved fluid system, which would correspond to the transitional magmatic–hydrothermal stage.

Based on the crustal origin of the parental magma with little or no contribution from the mantle (deduced from the Lu–Hf isotopes, Embui et al. 2020), we infer that the melt evolved from a starting composition close to the average continental crust, which must have δ^{98}Mo values between that reported for Phanerozoic upper continental crust (0.14 ± 0.07 ‰; Yang et al. 2017) and mantle (0.04 ± 0.07 ‰: Greber et al. 2015).

Fractional crystallization of the melt system produced a sequence of rocks from biotite granite through biotite–

Fig. 6. Box plot of δ^{98}Mo values of molybdenite from granite, pegmatite and a quartz–muscovite vein in the Ekomédion prospect. Note that molybdenite in pegmatite tends to have heavier δ^{98}Mo signatures than in granite whereas the molybdenite from the quartz–muscovite vein exhibits the isotopically heaviest Mo.
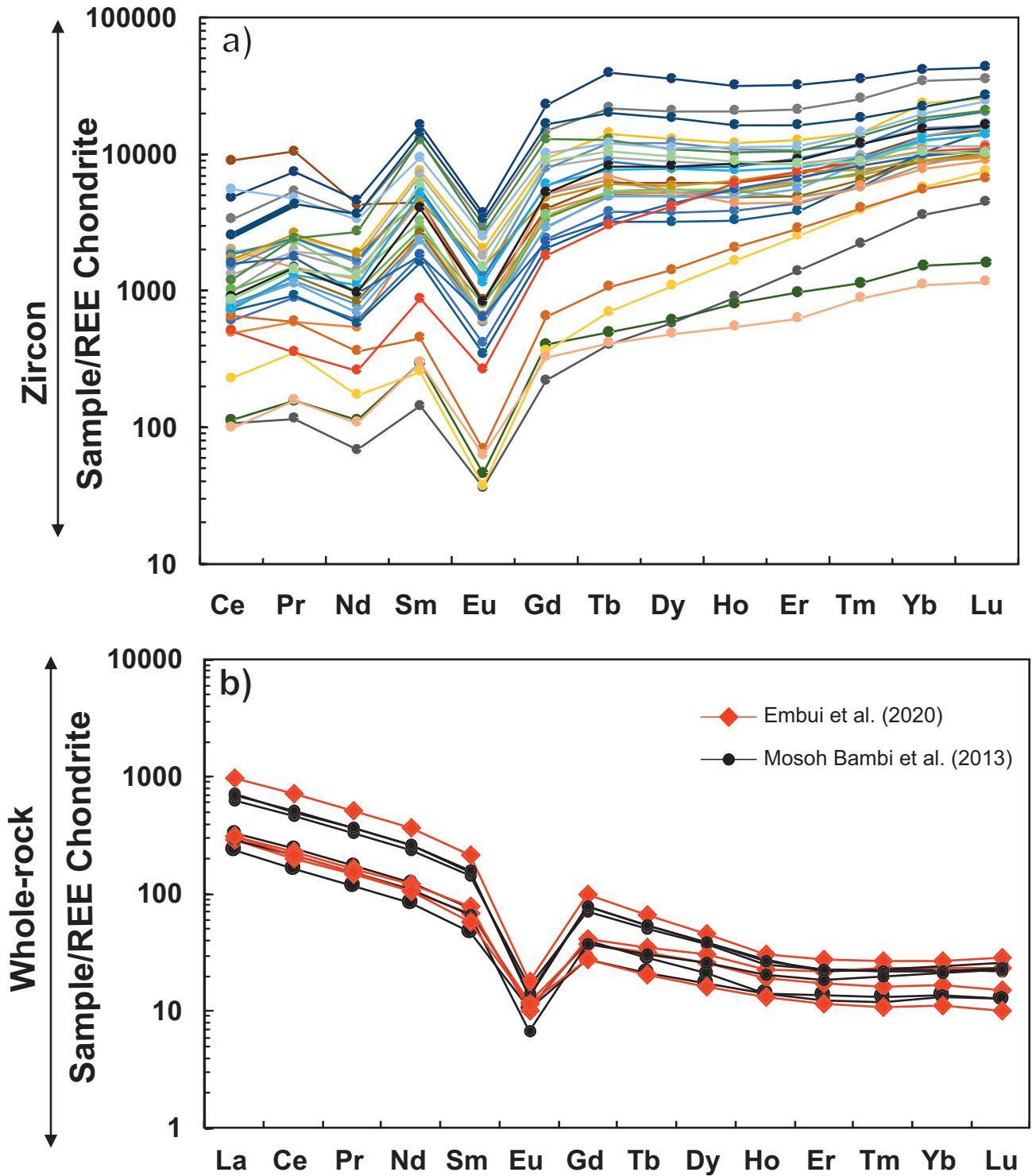
Fig. 7. Chondrite-normalized (Sun and McDonough 1989) rare earth element plots for zircon (a) and (b) whole-rock. Data for zircon from Embui et al. (2020), data for whole-rock chemistry from Embui et al. (2020) and Mosoh Bambi et al. (2013). Both zircon and whole-rock samples reveal a distinct negative Eu anomaly.

muscovite granite to pegmatite. The interpretation of the biotite granite to pegmatite sequence as due to fractional crystallization is in agreement with the overlapping molybdenite Re–Os ages (578 ± 11 Ma and 577 ± 11 Ma) determined for both granite- and pegmatite-related mo-

lybdenite from the Ekomédion prospect (Mosoh Bambi et al. 2013). Furthermore, the REE patterns of both zircon and whole-rock samples (Figs 7a–b) indicate a variable degree of plagioclase fractionation as inferred from the negative Eu anomalies. Based on bulk-rock geochemistry,
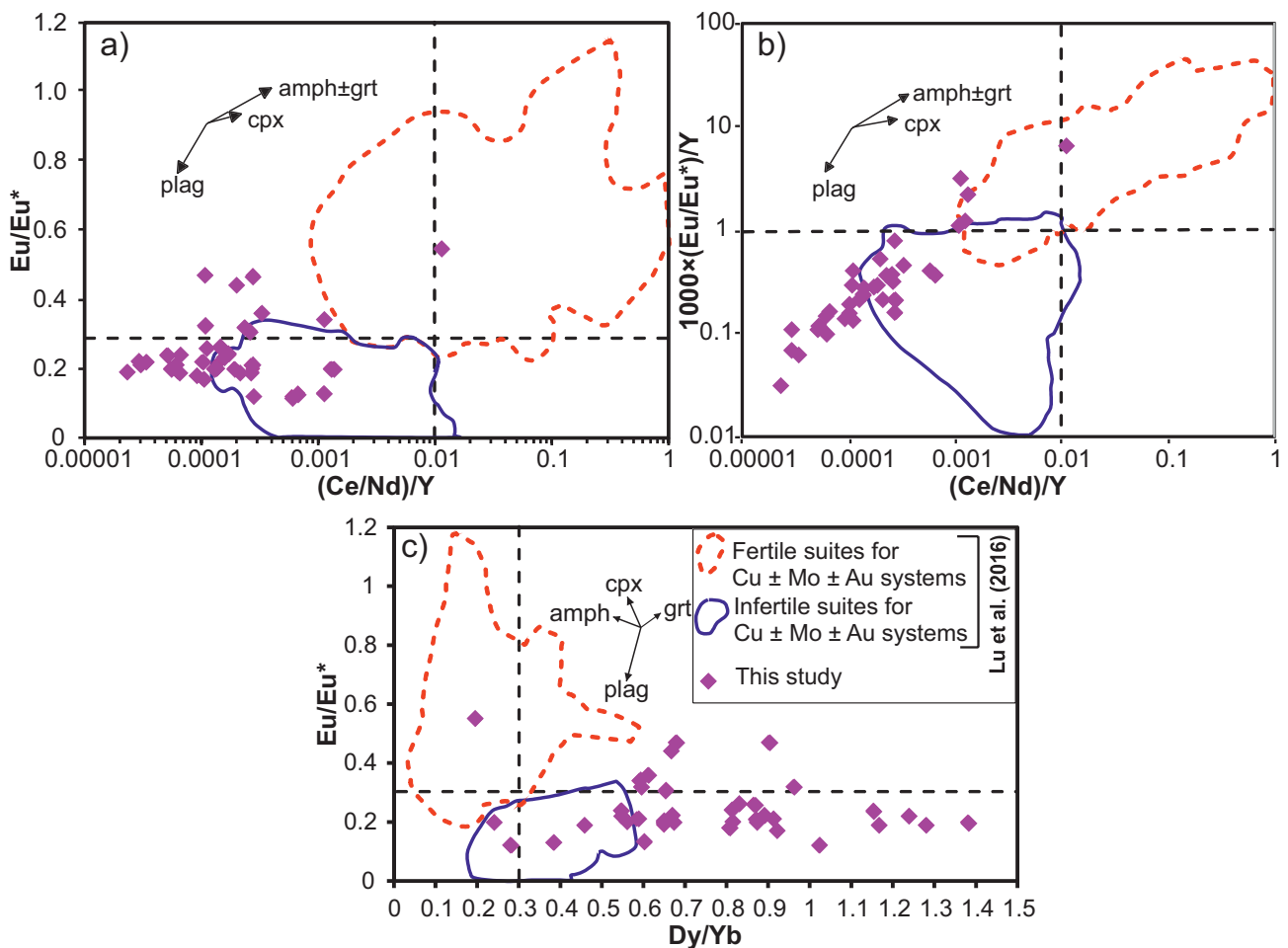
fractional crystallization of the granitic rocks in the Ekomédion area has previously been documented in detail in the work of Embui et al. (2020).

Molybdenum isotope fractionation during fractional crystallization has been documented in arc systems (Greber et al. 2014; Voegelin et al. 2014; Wille et al. 2018). Such Mo isotope fractionation would enrich isotopically heavier Mo in residual melts, and the slight shift in $\delta^{98}Mo$ values of molybdenite from biotite–muscovite granite (0.03 ± 0.07 ‰; n = 4) to pegmatite (0.11 ± 0.10 ‰; n = 5) could reflect this behavior. When Mo partitions from hydrous silicate melt into the exsolving hydrothermal fluid phase, isotope fractionation towards heavier Mo occurs (Greber et al. 2014).

The molybdenite samples from disseminations/veinlets and pods have a little fractionated Mo isotope signature and must be relatively close to the igneous Mo isotope composition. In fact, they likely represent a relatively closed system, given the pod-like appearance reminiscent of miarolitic cavities. During fluid evolution, such as in larger vein systems, molybdenite progressively

becomes isotopically heavier because isotopically light Mo partitions preferentially into molybdenite, similar to the behaviour of silicate phases in the igneous system (Greber et al. 2014; Voegelin et al. 2014). The isotope fractionation becomes more pronounced with decreasing temperature (Kaufmann et al. 2021).

Kaufmann et al. (2021) provided data for Mo isotope fractionation in a magmatic–hydrothermal system involving analyses of minerals, bulk rock and fluid. Their data suggest that significant fractionation effects can arise during magmatic–hydrothermal processes in which Mo isotope evolution commences with Mo transfer into the fluid phase exsolving from the solidifying magma during late-stage igneous evolution. This depletes the bulk rock, in our case, the two-mica granite, of isotopically heavy Mo, and is followed by the precipitation of hydrothermal minerals from the cooling fluids, which will preferentially incorporate light Mo isotopes (Kaufmann et al. 2021). Consequently, the remaining fluid evolves towards increasingly heavier Mo. The quartz vein sample in our study represents such a late-stage

Fig. 8. Variation diagrams for trace-element ratios of zircon from two-mica granite sample CMR09 in Embui et al. (2020): a) Eu/Eu* vs. (Ce/Nd)/Y, b) 10000 × (Eu/Eu*)/Y vs. (Ce/Nd)/Y and c) Eu/Eu* vs. Dy/Yb compared to the data of Lu et al. (2016). Ekomédion data illustrate a a dominant plagioclase fractionation and little potential for magmatic–hydrothermal ore deposits of the Cu–Mo–Au spectrum.

situation with molybdenite of an isotopically heavy composition of 1.61‰ $\delta^{98}Mo$.

5.2. Fertility of the Ekomédion granite system inferred from zircon and whole-rock trace-element chemistry

Previously published LA–ICP–MS trace-element concentrations of zircon from a two-mica granite sample within the Mo–U prospect (Embui et al. 2020) show that the U concentrations are highly variable and range from 155 ppm to 19600 ppm. The most elevated U and Th contents of zircon (>1000 ppm U, >1000 ppm Th) are the reason why the U–Pb ages of zircon are disturbed (Embui et al. 2020). Rare earth element contents are also highly variable, with elevated REE (>100 ppm Ce) in the high-U zircons (>1000 ppm U). Chondrite-normalized REE plots are characterized by distinctly negative Eu anomalies (Fig. 7a).

Collectively, the negative Eu anomaly with Eu/Eu* ranging from 0.12–0.26 and 0.12–0.29 for zircon and whole-rock samples, respectively (Figs 7a–b), can be interpreted to reflect a reducing melt that allowed the early formation of plagioclase. Plagioclase sequestered Eu^{2+} through substitution for Ca^{2+}, leaving the remaining melt poor in Eu and resulting in deep negative Eu anomalies in both zircon and its granitic host rocks.

Studies by Loucks (2014) and Shen et al. (2015) have shown that oxidized magmas provide favorable conditions for the mineralization of metals such as Mo, Cu and Au by inhibiting early sulfide precipitation. This allows the ore metals to be concentrated in the residual melt and hydrothermal fluids. By comparison, the accessory ilmenite present in the Ekomédion granitic rocks indicates reducing melt conditions, unfavorable for Mo mineralization (Ishihara 1981).

Tab. 2. Calculated ratios of Eu/Eu*, 10000 × (Eu/Eu*)/Y, Ce_N/Ce_N* and Dy/Yb for zircon from Ekomédion

Sample ID	Eu/Eu*	10000×(Eu/Eu*)/Y	Ce_N/Ce_N*	Dy/Yb
CM_1	0.22	0.23	3.13	0.55
CM_2	0.55	6.48	19.35	0.20
CM_4	0.47	0.80	3.00	0.68
CM_5	0.20	0.21	4.53	0.88
CM_6	0.17	0.19	2.29	0.92
CM_7	0.24	0.11	3.32	0.81
CM_8	0.20	0.29	2.93	0.56
CM_9	0.26	0.28	2.91	0.87
CM_10	0.19	0.32	3.40	0.46
CM_11	0.20	0.20	2.14	0.67
CM_12	0.20	1.22	3.23	0.24
CM_14	0.20	0.24	2.73	0.82
CM_15	0.19	0.03	3.71	1.28
CM_16	0.34	3.16	3.07	0.59
CM_17	0.13	1.12	2.53	0.60
CM_18	0.24	0.28	3.70	0.55
CM_19	0.12	0.16	6.16	1.02
CM_20	0.24	0.16	2.94	1.15
CM_21	0.12	0.41	1.94	0.28
CM_22	0.19	0.10	3.14	1.17
CM_23	0.19	0.21	3.52	0.65
CM_24	0.22	0.16	3.44	0.67
CM_25	0.13	0.37	2.22	0.38
CM_26	0.22	0.06	3.12	0.89
CM_27	0.32	0.29	2.17	0.96
CM_28	0.31	0.37	3.11	0.65
CM_29	0.21	0.11	2.07	0.87
CM_30	0.26	0.13	4.67	0.83
CM_31	0.47	0.40	2.35	0.90
CM_32	0.20	2.24	2.49	0.65
CM_33	0.21	0.15	3.09	0.91
CM_34	0.21	0.22	6.52	0.58
CM_35	0.18	0.14	3.81	0.81
CM_36	0.20	0.12	3.23	1.38
CM_37	0.44	0.52	2.83	0.67
CM_38	0.32	0.37	4.18	0.59
CM_39	0.22	0.07	2.68	1.24
CM_40	0.36	0.45	0.59	0.61

Primary data for these calculations can be found in Embui et al. (2020).

Several studies have shown that Eu/Eu* > 0.3 and 10,000 × (Eu/Eu*)/Y > 1 ratios in zircon, as well as (Ce/Nd)/Y > 0.01 and Dy/Yb < 0.3 in whole-rock are useful fertility indicators for the Cu–Mo–Au spectrum (Dilles et al. 2015; Lu et al. 2016; Li et al. 2019). Such distinct zircon trace-element ratios are interpreted to indicate an anomalous differentiation trend in thickened continental crust, i.e., suppression of plagioclase fractionation and enhanced early amphibole fractionation. This reflects high magmatic water content, which is favorable for magmatic–hydrothermal (porphyry-style) ore formation. Our data indicate significant plagioclase fractionation and little or no amphibole fractionation in the magmatic

evolution of the Ekomédion granite magmatism. Our data (Tab. 2) plot mainly outside the fertile fields as defined by Lu et al. (2016) (Figs 8a–c), supporting dominantly plagioclase fractionation in a reduced and less hydrous melt system.

Plagioclase versus amphibole fractionation imprint is further expressed in trace-element characteristics of the bulk rock, such as elevated V/Sc. Scandium preferentially partitions into amphibole and the suppression of magnetite in a more hydrous, oxidized melt leads to enrichment in V (Loucks 2014; Lu et al. 2018). The low V/Sc ratios observed in the Ekomédion granitic rocks suggest plagioclase fractionation dominantly, as also observed in the zircon trace-element chemistry (Fig. 8). In addition to the low whole-rock V/Sc ratios, Sr/Y ratios are also low (1.7–6.5; Embui et al. 2020), which is interpreted as a characteristic of the granites generated from the melting of the average lower or middle crust within the plagioclase-stable field, i.e., at a crustal depth of fewer than 40 km (Richards 2011; Moyen and Martin 2012; Villela Cassini et al. 2021). The molybdenite from Ekomédion also has meager Re contents (1–2 ppm Re; Mosoh Bambi et al. 2013), which is typical of crustal-derived disseminated molybdenite mineralization in granite and Sn–W deposits (Pašava et al. 2016). But this is significantly lower than reported for all major Mo ore deposits, re-iterating a low Mo potential (Barton et al. 2020).

6. Conclusions

- The molybdenum isotope composition of molybdenite from the Ekomédion prospect, Cameroon reveals that molybdenite formed from magmatic–hydrothermal fluids that exsolved from felsic magma that underwent fractional crystallization.
- Zircon, as well as whole-rock trace-element chemistry, provide clues on the fertility of the Ekomédion granite system. The new data collectively argue that the observed granitic intrusions are of low fertility potential concerning Mo because of reducing melt conditions typical of ilmenite-series granites.
- Plagioclase fractionation is depicted by both zircon and whole-rock REE patterns, characterized by negative Eu anomalies. The zircon Eu/Eu*, (Eu/Eu*)/Y, (Ce/Nd)/Y and Dy/Yb ratios are different from those typical of amphibole fractionation which characterize Cu–Mo–Au ore systems.

References

Asaah VA, Basem Z, Lehmann B, Frei D, Burgess R, Suh CE (2015) Geochemistry and geochronology of the ~620 Ma gold-associated Batouri granitoids, Cameroon. Int Geol Rev 57: 1485–1509

Ateh KI, Suh CE, Shemang EM, Vishiti A, Tata E, Chombong NN (2017) New LA-ICP-MS U–Pb ages, Lu–Hf systematics and REE characterization of zircons from a granitic pluton in the Bétaré Oya gold district, SE Cameroon. Int J Geomat Geosci 5: 267–283

Ballard JR, Palin JM, Campbell IH (2002) Relative oxidation states of magmas inferred from Ce(IV)/Ce(III) in zircon: application to porphyry copper deposits of northern Chile. Contrib Mineral Petrol 144: 347–364

Barling J, Arnold GL, Anbar AD (2001) Natural mass-dependent variations in the isotopic composition of molybdenum. Earth Planet Sci Lett 19: 447–457

Barton IF, Rathkopf CA, Barton MD (2020) Rhenium in molybdenite: a database approach to identifying geochemical controls on the distribution of a critical element. Mining Metall Explor 37: 21–37

Blevin PL (2004) Redox and compositional parameters for interpreting the granitoid metallogeny of eastern Australia: implications for gold-rich ore systems. Resour Geol 54: 241–252

Breillat N, Guerrot C, Marcoux E, Négrel P (2016) A new global database of δ⁹⁸Mo in molybdenites: a literature review and new data. J Geochem Explor 161: 1–15

Caen-Vachette M, Vialette Y, Bassot JP, Vidal P (1988) Apport de la geochronology à la connaissance de la géologie gabonaise. Chronique de la recherche Minière 491: 35–54

Castaing C, Feybesse JL, Thieblemont D, Triboulet C, Chevremont P (1994) Palaeogeographical reconstructions of the Pan-African/Brasiliano Orogen: closure of an oceanic domain or intracontinental convergence between major blocks. Precambr Res 69: 327–344

Chang J, Li JW, Zhou L (2020) Molybdenum isotopic fractionation in the Tibetan Yulong Cu–Mo deposit and its implications for mechanisms of molybdenite precipitation in porphyry ore systems. Ore Geol Rev 123: 103–571

Chen YJ, Li C, Zhang J, Li Z, Wang HH (2002) Sr and O isotopic characteristics of porphyries in the Qinling molybdenum deposit belt and their implication to genetic mechanism and type. Sci China Ser D, Earth Sci 43: 82e94

Chombong NN, Suh CE (2013) 2883 Ma commencement of BIF deposition at the northern edge of Congo Craton, southern Cameroon: new zircon SHRIMP data constraint from metavolcanics. Episodes 36: 47–57

CHOMBONG NN, SUH CE, LEHMANN B, VISHITI A, ILOUG DC, SHEMANG EM, TANTOH BS, KEDIA AC (2017) Host rock geochemistry, texture and chemical composition of magnetite in iron ore in the Neoarchaean Nyong Unit in southern Cameroon. Appl Earth Sci 126: 129–145

DILLES JH, KENT AJR, WOODEN JL, TOSDAL RM, KOLESZAR A, LEE RG, FARMER LP (2015) Zircon compositional evidence for sulfur degassing from ore-forming arc magmas. Econ Geol 110: 241–251

DJOUKA-FONKWE ML, SCHULZ B, SCHÜSSLER U, TCHOUANKOUE JP, NZOLANG C (2008) Geochemistry of the Bafoussam Pan-African I- and S-type granitoids in western Cameroon. J African Earth Sci 50: 148–167

EMBUI VF, SUH CE, COTTLE JM, ETAME J, MENDES J, AGYINGI CM, VISHITI A, SHEMANG EM, LEHMANN B (2020) Zircon chemistry and new laser ablation U–Pb ages for uraniferous granitoids in SW Cameroon. Acta Geochem 39: 43–66

GASPERS N, MAGNA T, ACKERMAN L (2020) Molybdenum mass fractions and stable isotope compositions of sedimentary carbonate and silicate reference materials. Geostand Geoanal Res 44: 363–374

GREBER ND, HOFMANN BA, VOEGELIN AR, VILLA IM, NÄGLER TF (2011) Mo isotope composition in Mo-rich high- and low-T hydrothermal systems from the Swiss Alps. Geochim Cosmochim Acta 75: 6600–6609

GREBER ND, PETTKE T, NÄGLER TF (2014) Magmatic–hydrothermal molybdenum isotope fractionation and its relevance to the igneous crustal signature. Lithos 190–191: 104–110.

GREBER NB, PUCHTEL IS, NÄGLER TF, MEZGER K (2015) Komatiites constrain molybdenum isotope composition of the Earth's mantle. Earth Planet Sci Lett 421: 129–138

HANNAH JL, STEIN HJ, WIESER ME, DE LAETER JR, VARNER MD (2007) Molybdenum isotope variations in molybdenite: vapor transport and Rayleigh fractionation of Mo. Geology 35: 703–706

ISHIHARA S (1981) The granitoid series and mineralization. Econ Geol 75th Anniversary Volume: 458–484

JOHNSON CM, BEARD BL (2006) Fe isotopes; an emerging technique for understanding modern and ancient biogeochemical cycles. GSA Today 16: 4–10

KANKEU B, GREILING RO (2006) Magnetic fabrics (AMS) and transpression in the Neoproterozoic basement of eastern Cameroon (Garga-Sarali area). Neu Jb Geol Paläont, Abh 239: 263–287

KANKEU B, GREILING RO, NZENTI JP (2009) Pan-African strike-slip tectonics in eastern Cameroon: magnetic fabrics (AMS) and structures in the Lom basin and its gneissic basement. Precambr Res 174: 258–272

KAUFMANN CKA, PETTKE T, WILLE M (2021) Molybdenum isotope fractionation at upper-crustal magmatic–hydrothermal conditions. Chem Geol 578: 120319

KENDALL B, DAHL TW, ANBAR AD (2017) The stable isotope geochemistry of molybdenum. In:-TENG FZ, WATKINS J, DAUPHAS N (eds) Non-Traditional Stable Isotopes. Rev Mineral Geochem 82: 683–732

LEROUGE C, COCHERIE A, TOTEU SF, PENAYE J, MILÉSI JP, TCHAMENI R, NSIFA EN, FANNING CM, DELOULE E (2006) SHRIMP U–Pb zircon age evidence for Paleoproterozoic sedimentation and 2.05 Ga syntectonic plutonism in the Nyong Group, south-western Cameroon: consequences for the Eburnean–Transamazonian belt of NE Brazil and Central Africa. J African Earth Sci 44: 413–427

LI CY, WANG FY, HAO XL, DING X, ZHANG H, LING MX, ZHOU JB, LI YL, FAN WM, SUN WD (2012) Formation of the world's largest molybdenum metallogenic belt: a plate-tectonic perspective on the Qinling molybdenum deposits. Int Geol Rev 54: 1093–1112

LI HX, CHEN Y, TCHOUANKOUE JP, LIU CZ, LI J, LING XX, TANG GQ, LIU Y (2017) Improving geochronological framework of the Pan-African Orogeny in Cameroon: new SIMS zircon and monazite U–Pb age constraints. Precambr Res 379: 307–321

LI Y, MCCOY-WEST AJ, ZHANG S, SELBY D, BURTON KW, HORAN K (2019) Controlling mechanisms for molybdenum isotope fractionation in porphyry deposits: the Qulong example. Econ Geol 114: 981–992

LOUCKS RR (2014) Distinctive composition of copper-ore-forming arc magmas. Austr J Earth Sci 61: 5–16

LU YJ, LOUCKS RR, FIORENTINI M, MCCUAIG TC, EVANS NJ, YANG ZM, HOU ZQ, KIRKLAND CL, PARRA-AVILA LA, KOBUSSEN A (2016) Zircon compositions as a pathfinder for porphyry Cu±Mo±Au deposits. In: RICHARDS JP (ed) Tectonics and Metallogeny of the Tethyan Orogenic Belt. Society of Economic Geologists, Special Publication 19: 329–347

LU YJ, SMITHIES RH, WINGATE MTD, EVANS NJ, MORRIS, PA, CHAMPION DC, MCCUAIG TC (2018) Zircon composition as a fertility indicator of Archean granites. In: GSWA 2018 Extended Abstracts: Promoting the Prospectivity of Western Australia. Geological Survey of Western Australia Records 2018/2: 18–23

MATHUR R, BRANTLEY S, ANBAR A, MUNIZAGA F, MAKSAEV V, NEWBERRY R, VERVOORT J, HART G (2010) Variation of Mo isotopes from molybdenite in high-temperature hydrothermal ore deposits. Miner Depos 45: 43–50

MOSOH BAMBI CK, SUH CE, NZENTI JP, FRIMMEL HE (2012) U–Mo mineralization potential in Pan-African granites, southwestern Cameroon: economic geology of the Ekomédion prospect. J African Earth Sci 65: 25–45

MOSOH BAMBI CK, FRIMMEL HE, ZEH A, SUH CE (2013) Age and origin of Pan-African granites and associated U–Mo mineralization at Ekomédion, southwestern Cameroon. J African Earth Sci 88: 15–37

MOYEN JF, MARTIN H (2012) Forty years of TTG research. Lithos 148: 312–336

NÄGLER TF, ANBAR AD, ARCHER C, GOLDBERG T, GORDON GW, GREBER ND, SIEBERT C, SOHRIN Y, VANCE D (2014)

Proposal for an international molybdenum isotope measurement standard and data representation. Geostand Geoanal Res 38: 149–151

Neves SP, Silva JMR, Mariano G (2005) Oblique lineations in orthogneisses and supracrustal rocks: vertical partitioning of strain in a hot crust (eastern Borborema Province, NE Brazil). J Struct Geol 27: 1507–1521

Ngako V, Affaton P, Njonfang E (2008) Pan-African tectonics in northwestern Cameroon: implication for the history of western Gondwana. Gondwana Res 14: 509–522

Njome MS, Suh CE (2005) Tectonic evolution of the Tombel Graben basement, south western Cameroon. Episodes 28: 37–41

Pašava J, Svojtka M, Veselovský F, Ďurišová J, Ackerman L, Pour O, Drábek M, Halodová P, Haluzová E (2016) Laser ablation ICPMS study of trace element chemistry in molybdenite coupled with scanning electron microscopy (SEM) – an important tool for identification of different types of mineralization. Ore Geol Rev 72: 874–895

Penaye J, Kröner A, Toteu SF, Van-Schmus WR, Doumnang JC (2006) Evolution of the Mayo Kebbi region as revealed by zircon dating: an early (c. 740 Ma) Pan-African magmatic arc in southwestern Chad. J African Earth Sci 44: 530–542

Pouclet A, Tchameni R, Mezger K, Vidal M, Nsifa EN, Shang CK, Penaye J (2007) Archean crustal accretion at the northern border of the Congo Craton (South Cameroon): the charnockite–TTG link. Bull Soc Géol France 178: 331–342

Richards JP (2011) High Sr/Y arc magmas and porphyry Cu ± Mo ± Au deposits: just add water. Econ Geol 106: 1075–1081

Shafiei B, Shamanian G, Mathur R, Mirnejad H (2015) Mo isotope fractionation during hydrothermal evolution of porphyry Cu systems. Miner Depos 50: 281–291

Shen P, Hattori K, Pan H, Jackson S, Seitmuratova E (2015) Oxidation condition and metal fertility of granitic magmas: zircon trace-element data from porphyry Cu deposits in the Central Asian Orogenic Belt. Econ Geol 110: 1861–1878

Sun SS, McDonough WF (1989) Chemical and isotopic systematics of oceanic basalts: implications for mantle composition and processes. In: Saunders AD, Norry MJ (eds) Magmatism in the ocean basins. Geological Society of London Special Publications 42: 313–345

Sun WD, Li CY, Hao XL, Ling MX, Ireland T, Ding X Fan WM (2015) Oceanic anoxic events, subduction style and molybdenum mineralization. Solid Earth Sci 1: 64–73

Tagne-Kamga G (2003) Petrogenesis of the Neoproterozoic Ngondo Plutonic Complex (Cameroon, west central Africa); a case of late-collisional ferro-potassic magmatism.

J African Earth Sci 36: 149–171

Tita MA, Kaya M (2020) Minerals in Cameroon. ESOGU–CHTP. http://dx.doi.org/10.13140/RG.2.2.19764.88968

Toteu SF, Penaye, J, Deloule E, Van Schmus WR, Tchameni R (2006) Diachronous evolution of volcano-sedimentary basins north of the Congo Craton: insights from U–Pb ion microprobe dating of zircons from the Poli, Lom and Yaounde Series (Cameroon). J African Earth Sci 44: 428–442

Trompette R (1997) Neoproterozoic (600 Ma) aggregation of Western Gondwana: a tentative scenario. Precambr Res 82: 101–112

Van-Schmus WR, Oliveira EP, Silva DA, Filho AF, Toteu SF, Penaye J, Guimarães, IP (2008) Proterozoic links between the Borborema Province, NE Brazil, and the Central African Fold Belt. In: Pankhurst RJ, Trouw RAJ, de Brito Neves BB, de Wit MJ (eds) West Gondwana. Geological Society of London Special Publications 294: 69–99

Villela Cassini L, Moyen JF, Cellier G, de Freitas B, Juliani C, Laurent O (2021) Towards the fertility trend: unravelling the economic potential of igneous suites through whole-rock and zircon geochemistry (example from the Tapajós Mineral Province, northern Brazil). Ore Geol Rev 142: 104–643

Voegelin AR, Pettke T, Greber ND, von Niederhausern B, Nägler TF (2014) Magma differentiation fractionates Mo isotope ratios: evidence from the Kos Plateau Tuff (Aegean Arc). Lithos 190: 440–448

Willbold M, Elliott T (2017) Molybdenum isotope variations in magmatic rocks. Chem Geol 449: 253–268

Wille M, Nebel O, Pettke T, Vroon ZP, König S, Schoenberg R (2018) Molybdenum isotope variations in calc-alkaline lavas from the Banda Arc, Indonesia: assessing the effect of crystal fractionation in creating isotopically heavy continental crust. Chem Geol 485: 1–13

Yang J, Barling J, Siebert C, Fietzke J, Stephens E, Halliday AN (2017) The molybdenum isotopic compositions of I-, S- and A-type granitic suites. Geochim Cosmochim Acta 205: 168–186

Yao J, Mathur R, Sun W, Song W, Chen H, Mutti L, Xiang X, Luo X (2016) Fractionation of Cu and Mo isotopes caused by vapor-liquid partitioning, evidence from the Dahutang W–Cu–Mo ore field. Geochem Geophys Geosyst 17: 1725–1739

Zhang H, Li CY, Yang XY, Sun YL, Deng JH, Liang HY, Wang RL, Wang BH, Wang YX, Sun WD (2014) Shapinggou: the largest Climax-type porphyry Mo deposit in China. Int Geol Rev 56: 313–331

Zhang L, Chen Y, Zhang R, Wang K, Luo Y, Li C, Liang J (2022) The Jurassic Gangmei Mo–W deposit in Guangdong Province and its implication for Mo–W mineralization in South China. Solid Earth Sci 7: 126–134